Bone 76 (2015) 23–30

Contents lists available at ScienceDirect

Bone

journal homepage: www.elsevier.com/locate/bone

Original Full Length Article

Osteoblast function and bone histomorphometry in a murine model of Rett syndrome

Mary E. Blue [a,*], Adele L. Boskey [b], Stephen B. Doty [b], Neal S. Fedarko [c], Mir Ahamed Hossain [a], Jay R. Shapiro [a]

[a] Hugo W. Moser Research Institute at Kennedy Krieger, Inc., 707 North Broadway, Baltimore, MD 21205, USA
[b] Hospital for Special Surgery, Mineralized Tissue Laboratory 535 E 70th Street, New York, NY 10021, USA
[c] Geriatric Medicine and Gerontology, Johns Hopkins Medical Institutions, Room 1A-12 JHAAC, 5501 Hopkins Bayview Circle, Baltimore, MD 21224, USA

ARTICLE INFO

Article history:
Received 1 August 2014
Revised 21 January 2015
Accepted 25 January 2015
Available online 10 March 2015

Edited by J. Aubin

Keywords:
Rett syndrome
Bone histology
MeCP2
Micro-CT
Osteoblast
Osteoclast

ABSTRACT

Rett syndrome (RTT) is an X-linked neurodevelopmental disorder due to mutations affecting the neural transcription factor MeCP2. Approximately 50% of affected females have decreased bone mass. We studied osteoblast function using a murine model of RTT. Female heterozygote (HET) and male *Mecp2*-null mice were compared to wild type (WT) mice. Micro-CT of tibia from 5 week-old *Mecp2*-null mice showed significant alterations in trabecular bone including reductions in bone volume fraction (−29%), number (−19%), thickness (−9%) and connectivity density (−32%), and increases in trabecular separation (+28%) compared to WT. We also found significant reductions in cortical bone thickness (−18%) and in polar moment of inertia (−45%). In contrast, cortical and trabecular bone from 8 week-old WT and HET female mice were not significantly different. However, mineral apposition rate, mineralizing surface and bone formation rate/bone surface were each decreased in HET and *Mecp2*-null mice compared to WT mice. Histomorphometric analysis of femurs showed decreased numbers of osteoblasts but similar numbers of osteoclasts compared to WT, altered osteoblast morphology and decreased tissue synthesis of alkaline phosphatase in *Mecp2*-null and HET mice. Osteoblasts cultured from *Mecp2*-null mice, which unlike WT osteoblasts did not express MeCP2, had increased growth rates, but reductions in mRNA expression of *type I collagen*, *Runx2* and *Osterix* compared to WT osteoblasts. These results indicate that MeCP2 deficiency leads to altered bone growth. Osteoblast dysfunction was more marked in *Mecp2*-null male than in HET female mice, suggesting that expression of MeCP2 plays a critical role in bone development.

© 2015 Elsevier Inc. All rights reserved.

Introduction

Rett (RTT) syndrome is a neurodevelopmental disorder affecting worldwide ~1 in 10,000 young females and a smaller number of males [1]. RTT is most often caused by loss of function mutations in the X-linked gene Methyl CpG binding protein (*MECP2*) located at Xq28, encoding methyl-CpG-binding protein 2 (MeCP2) [2]. The murine gene and transcription factor proteins are designated *Mecp2* and MeCP2 respectively. MeCP2 is a global transcriptional regulatory protein with both gene repressor and activator functions [3,4].

Diminished bone mass with lumbar spine bone density Z-scores between −1.5 and −2 SD, or lower than −2 SD below the mean for age, is a well-recognized complication of RTT [5,6]. The reported incidence of low bone mass approximates 50% in young individuals with RTT [7]. This may be evident by 4–6 years of age. At the Kennedy Krieger Institute, approximately 11% of individuals with RTT have suffered fractures. Other reports confirm an increased fracture rate in Rett [8,9]. Although use of anti-seizure medication, poor nutrition and impaired ambulation independently affect bone mass, these factors cannot entirely explain the early onset and increased incidence of osteoporosis in children with RTT. The pathogenesis of decreased bone mass in RTT is not fully understood. Histological studies in murine models and bone biopsies from a small series of patients suggest that *MECP2* mutations impair bone formation [10,11]. However, the effects of *MECP2* mutations on bone cell function have not been fully defined. This report addresses alterations in osteoblasts and osteoclasts as well as static and dynamic parameters in the Adrian Bird murine model of MeCP2 deficiency [12].

Abbreviations: RTT, Rett syndrome; *MECP2*, Human gene for Methyl CpG binding protein; *Mecp2*, Mouse gene for Methyl CpG binding protein; MeCP2, Human and mouse protein Methyl CpG binding protein; *Mecp2*-null, Hemizygous male missing *Mecp2*; HET, Heterozygous female; WT, Wild type; TRAP, Tartrate resistance acid phosphatase; *Col1α1*, type I collagen alpha1 chain; BV/TV, Bone volume fraction; Tb.N, Trabecular number; Tb.Th, Trabecular thickness; Conn.D, Trabecular connectivity density; Tb.Sp, Trabecular separation; Ct.Th, Cortical thickness; pMOI, Polar moment of inertia; BMD, Bone mineral density; MAR, Mineral apposition rates; BFR/BS, Bone formation rates/surface; SD, Standard Deviation; XCI, X-chromosome inactivation.

* Corresponding author at: Room 400R, Kennedy Krieger Institute, 707 North Broadway, Baltimore, MD 21205, USA.
E-mail addresses: blue@kennedykrieger.org (M.E. Blue), BoskeyA@HSS.EDU (A.L. Boskey), DotyS@HSS.EDU (S.B. Doty), nfedark1@jhmi.edu (N.S. Fedarko), hossain@kennedykrieger.org (M.A. Hossain), shapiroj@kennedykrieger.org (J.R. Shapiro).

http://dx.doi.org/10.1016/j.bone.2015.01.024
8756-3282/© 2015 Elsevier Inc. All rights reserved.

Material and methods

Animals

These studies used a mouse model of MeCP2 deficiency developed in Adrian Bird's laboratory in which *Mecp2* exons 3 and 4 were deleted using Cre-lox methods [12]. *Mecp2*tm1.1Bird mice (Jackson Laboratory, Bar Harbor, Maine) were bred on a C57BL/6 background (heterozygote backcrossed with C57BL/6 males for at least nine generations). The Animal Care and Use Program at Johns Hopkins University approved our mouse study protocol.

Genotyping

The DNAeasy Blood & Tissue Kit was used for mice genotyping (Qiagen, Germantown, MD, USA). At 1 week of age, approximately 1–3 mm of tail was clipped and placed in individual sterile microcentrifuge tubes, rinsed in Qiagen buffer and DNA was extracted. Sample (1 ml) was added to each of primer cocktails containing the Mecp2 COMR (sequence GGTAAAGACCCATGTGACCC), *Mecp2* Wild Type (WT) female (sequence GGCTTGCCACATGACAA), and *Mecp2*-null (Mecp2-null) (sequence TCCACCTAGCCTGCCTGTAC) [13]. Each sample plus WT primer and *Mecp2*-null primer was run through 36 PCR cycles using an MJ Research DNA engine. Gel electrophoresis was performed using a 2% agarose + Sybr@safe gel (Life Technologies, Grand Island, NY).

Micro-CT

Mecp2-null mice have shortened lifespans compared to HET females, thus WT males and *Mecp2*-null mice were euthanized at 5–8 weeks of age and WT and HET females were euthanized at 8–12 weeks of age ($n = 5$ for each group). To prepare the bones for micro-CT and histological analyses, mice were sequentially injected with calcein and xylenol at days 5 and 3 respectively prior to euthanasia. Mice were anesthetized with choral hydrate prior to euthanasia by decapitation. The right and left femurs and tibias were excised and muscle and fascia were removed. For micro-CT, the tibias were placed in 70% ethanol and for histology the femurs were placed in 10% neutral buffered formalin. For micro-CT, three dimensional cancellous bone architecture and cortical bone geometry were determined at 12 μm voxel resolution (Scanco Micro-CT 35, Scanco Medical AG. Switzerland) as previously described [14]. Analyses and reconstructions were done with Scanco system software with specimen specific thresholds. Parameters measured were those recommended by ASBMR [15].

Histomorphology

Routine histomorphology and immunostaining were performed on femur and tibia metaphysis of WT, HET and *Mecp2*-null mice (5–7 animals/group; 3 sections/bone sample). For histological analyses of decalcified bone samples, the femurs and tibias were decalcified in 10% EDTA, 0.05 M Tris buffer, pH 7.4 until the bone was soft and flexible. Samples were processed (Sakura Tissue-Tek VIP processor), paraffin embedded and sectioned at 5 μm thickness. Slides were subsequently stained with alcian blue for cartilage, safranin O for proteolycans, picrosirius red for collagen, and H&E for standard morphometry and histology. Baseline measurements for bone volume and osteoblast numbers were performed only on secondary trabeculae excluding any trabeculae attached to growth plate and endosteum. Osteoblasts on secondary trabeculae were identified by immunostaining for type I procollagen. Osteoblast numbers were counted per 1 mm bone surface for *Mecp2*-null and WT male mice that were 5 weeks of age and for HET and WT female mice that were 12 weeks of age. Tartrate resistance acid phosphatase (TRAP) staining was used to identify osteoclasts. For TRAP staining, hexazonium pararosaniline was used for localization of acid phosphatase activity as described previously [16]. Tartrate is added to this phosphatase media to produce TRAP staining [17]. Using the standard TRAP stain on paraffin embedded sections, osteoclast counts were standardized by dividing the number of osteoclasts by surface perimeter, measured in millimeters. Osteoclasts were only evaluated along the secondary trabeculae; osteoclasts associated with the growth plate or primary trabeculae were not counted as these reflect bone remodeling that is largely related to the growth process.

For histology of calcified bone samples, formalin fixed femurs were embedded into polymethyl methacrylate according to the procedure of Erben [18]. Samples were sectioned on a Leica SM2500 sledge microtome using a carbon–tungsten blade. Sections, 5 μm thick, were stained with Goldners trichrome stain [19] to provide excellent cellular morphology and indicate new bone formation sites (osteoid). All histomorphometry was carried out using the Bioquant Osteo system (Bioquant Inc., Nashville, TN).

For alkaline phosphatase activity, paraffin sections were treated with 2 μg/ml protein kinase (37 °C, 30 min) for antigen retrieval, followed by rabbit polyclonal anti-alkaline phosphatase (Abcam 65834) overnight. Anti-rabbit IgG and ABC/diaminobenzene staining were used to visualize alkaline phosphatase (Vector Laboratories; Burlingame, CA). Hematoxylin was used as a counter stain for tissue definition. For labeling of osteoblasts, paraffin sections were stained with antibodies to procollagen type I. Sections were treated for antigen retrieval with hot sodium citrate buffer (20 min; 100 °C), incubated overnight with anti-procollagen I (SP1.D8, Developmental Studies Hybridoma Bank, Iowa City, Iowa), and visualized by the ABC/diaminobenzidine kit. Fluorochrome-based indices of bone formation were measured in unstained 5 μm longitudinal sections of distal femur. Double and single labeled perimeters were identified. Interlabel widths of double-labeled regions were measured using a Bioquant image analysis program. The mineral apposition rate (MAR, μm/day), mineralizing surface/bone surface (double label + 1/2 single label/total surface), and bone formation rates/surface (μ^3/μ^2/day) were then determined [20].

Cell culture

Excised femurs and tibias were cleaned of muscle, metaphyses from both ends were resected, and marrow components were eluted by flushing with a syringe and tissue culture medium. The bone was minced, treated with collagenase and an explant culture of the bone chips was propagated in DMEM containing 20% FBS and 2 mM glutamine and 50 μg/ml gentamycin. Subcultures of osteoblasts were seeded at 20,000 cells/cm^2 and grown in primary culture.

Growth curve analysis

Osteoblasts derived from long bones underwent growth curve analysis following fixation, staining with crystal violet and transformation of absorbance values to the natural logarithm of (time point absorbance/time zero absorbance). Growth curve profiling was carried out on WT mouse osteoblast cell lines ($n = 7$) and *Mecp2*-null osteoblast lines ($n = 8$). Growth curves were modeled by fitting each value versus time with a Zwietering modified logistic [21] using Prism software. The modeling determined the growth parameters: lag time, maximal growth rate and plateau value.

PCR

Semi-quantitative reverse transcriptase PCR was employed to analyze patterns of cellular phenotypic expression of the osteogenic transcription factors *Osterix* and *Runx2* and the osteoblast marker type I collagen alpha1 chain (*Col1α1*). Osteoblast strains derived from 3 WT and 3 *Mecp2*-null mice were plated at 20,000 cells/cm^2 and at each time point duplicate wells were harvested, RNA was extracted and

Table 1
Selected micro-CT parameters for trabecular and cortical bone in *Mecp2*-null male and HET female mice versus age-matched WT male and female mice. Micro-CT was performed on the tibia from 5 week-old *Mecp2*-null and WT male mice and 8 week-old HET and WT female mice (n = 5 for each group). The results indicate a marked alteration in bone from *Mecp2*-null mice compared to WT male mice.

	WT M	*Mecp2*-null M	WT F	HET F
Trabecular bone				
BV/TV	0.105 ± 0.006	0.075 ± 0.006*	0.113 ± 0.009	0.117 ± 0.006
BMD	826 ± 2	826 ± 4	870 ± 7	886 ± 5
Tb.N	6.370 ± 0.150	5.152 ± 0.268**	5.581 ± 0.197	5.668 ± 0.164
Tb.Th	0.023 ± 0.000	0.021 ± 0.000*	0.027 ± 0.001	0.029 ± 0.001*
Tb.Sp	0.155 ± 0.004	0.198 ± 0.011**	0.175 ± 0.006	0.170 ± 0.005
Conn.D	757 ± 63	512 ± 64*	550 ± 59	491 ± 36
Cortical bone				
BV/TV	0.494 ± 0.012	0.469 ± 0.011	0.540 ± 0.010	0.525 ± 0.010
BMD	988 ± 14	929 ± 12*	1037 ± 5	1023 ± 14
Ct.Th	0.133 ± 0.005	0.109 ± 0.002**	0.156 ± 0.002	0.150 ± 0.005
pMOI	0.060 ± 0.003	0.033 ± 0.004***	0.080 ± 0.009	0.077 ± 0.012

* $p < 0.05$.
** $p < 0.01$.
*** $p < 0.001$.

isolated (RNAzol, Sigma-Aldrich) and reverse transcriptase PCR was performed using the specific primers: *Osterix* = AGCGACCACTTGAGCA AACAT (sense) and GCGGCTGATTGGCTTCTTCT (antisense), *Runx2* = GCCGGGAATGATGAGAACTA (sense) and GGTGAAACTCTTGCCTCGTC (antisense), *Col1α1* = GCAACAGTCGCTTCACCTACA (sense) and CAAT GTCCAAGGGAGCCACAT (antisense) as described previously [22]. We ran the PCR in triplicate, with 3 gels to quantify the gene expression products. Values at each time point were normalized to the housekeeping gene *Gapdh*.

Statistical analysis

Statistical analysis for the micro-CT data and for the in vitro osteoblast cell counts was carried out using Prism GraphPad version 6.0 (GraphPad Software, Inc.). Since *Mecp2*-null and HET mice and their respective WT controls were analyzed at two different ages, t-tests were used to compare *Mecp2*-null versus WT male mice and HET versus WT female mice. To assess the effects of genotype on bone parameters, the data for each genotype was expressed as %WT and a repeated measures two-way analysis of variance and Holm-Sidak's multiple comparisons tests were performed with the repeated measures being different bone parameters for cortical and trabecular bone. Unpaired t-tests were used to compare WT and *Mecp2*-null cell growth parameters. Sigmaplot was used to statistically evaluate cell counts for osteoblasts and osteoclasts in histological sections. Group differences were compared by ANOVA or t-tests. Effects were considered significant at $p < 0.05$, and error bars indicate standard error of the mean.

Results

Micro-CT analysis

Micro-CT results from WT and *Mecp2*-null male mice showed significant alterations in a number of bone parameters for trabecular and cortical bone resulting from the absence of MeCP2. Due to the differences in the ages of the male and female mice, comparisons for individual parameters of trabecular and cortical bone were made by t-test. To assess the effects of genotype on bone parameters, to take into account the effects of multiple comparisons and to depict the results graphically, data for each genotype was expressed as %WT and a two-way analysis of variance was performed. For both trabecular and cortical bone, the results of the analysis showed significant effects for genotype ($p < 0.0001$ for both), bone parameter ($p < 0.0001$ for both) and interaction ($p < 0.05$ for trabecular bone and $p < 0.001$ for cortical bone) for the WT male versus *Mecp2*-null mice but not for WT versus HET female mice. The results showed significant reductions in trabecular bone volume fraction (BV/TV) (−29%), in trabecular number (Tb.N) (−19%), thickness (Tb.Th) (−9%) and connectivity density (Conn.D) (−32%) in *Mecp2*-null mice, while trabecular separation (Tb.Sp) was significantly increased (+28) compared to WT mice (Table 1, Fig. 1A). Cortical thickness (Ct.Th) (−18%) and polar moment of inertia (pMOI)

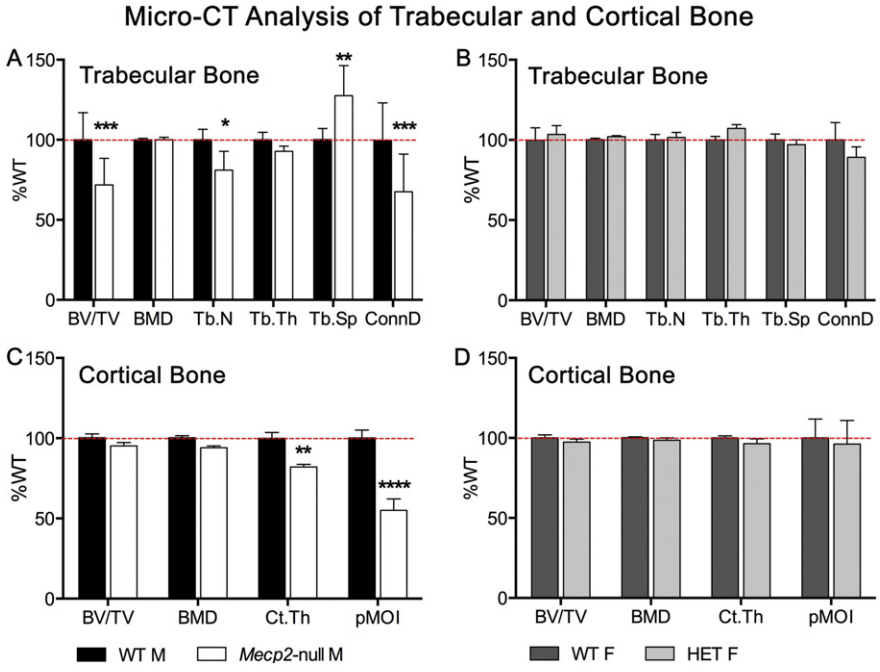

Fig. 1. Micro-CT studies show significant alterations in parameters for trabecular and cortical bone in *Mecp2*-null mice. Expression of the micro-CT data as %WT showed significant decreases in bone volume fraction (BV/TV), number (Tb.N) and connectivity density (Conn.D) of trabecular bone from *Mecp2*-null mice, while trabecular separation (Tb.Sp) increased (A; * = $p < 0.05$; ** = $p < 0.01$; *** = $p < 0.001$). In cortical bone of *Mecp2*-null mice, thickness (Ct.T) and polar moment of inertia (pMOI) were decreased (C; ****$p < 0.0001$). Trabecular (B) and cortical (D) bone parameters in HET mice did not differ from WT F mice. Values are the mean +/− standard error of the mean (SEM; n = 5 for each group).

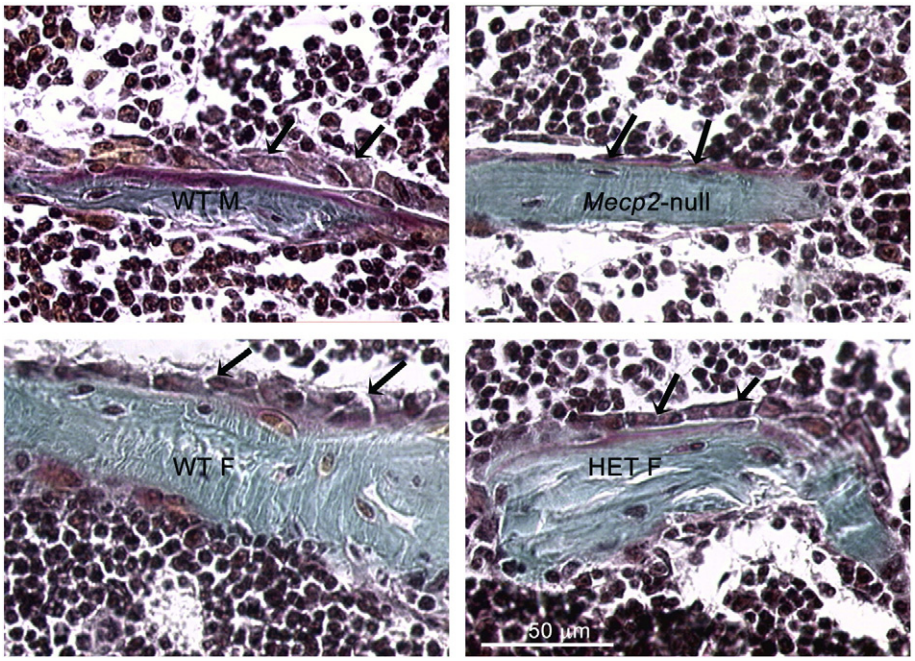

Fig. 2. Osteoblast morphology is altered in *Mecp2*-null mice. Osteoblasts from WT lining lamellae in deeper trabecular bone relative to the growth plate appear cuboidal while those of the *Mecp2*-null mice appear smaller and less plump. Black arrows demarcate osteoblasts. WT and *Mecp2*-null male mice were examined at 5 weeks of age. WT and HET female mice were examined at 12 weeks of age (5–7 mice were studied per group with 3 sections per bone sample examined).

(−45%) also were significantly decreased in *Mecp2*-null mice (Table 1, Fig. 1B). In contrast, cortical and trabecular bone in WT and HET female mice did not show any statistically significant differences in the bone parameters (Table 1, Figs. 1B, D).

Histomorphology

The initial examination of osteoblast histomorphology in *Mecp2*-null and WT male mice indicated that osteoblasts immediately under the

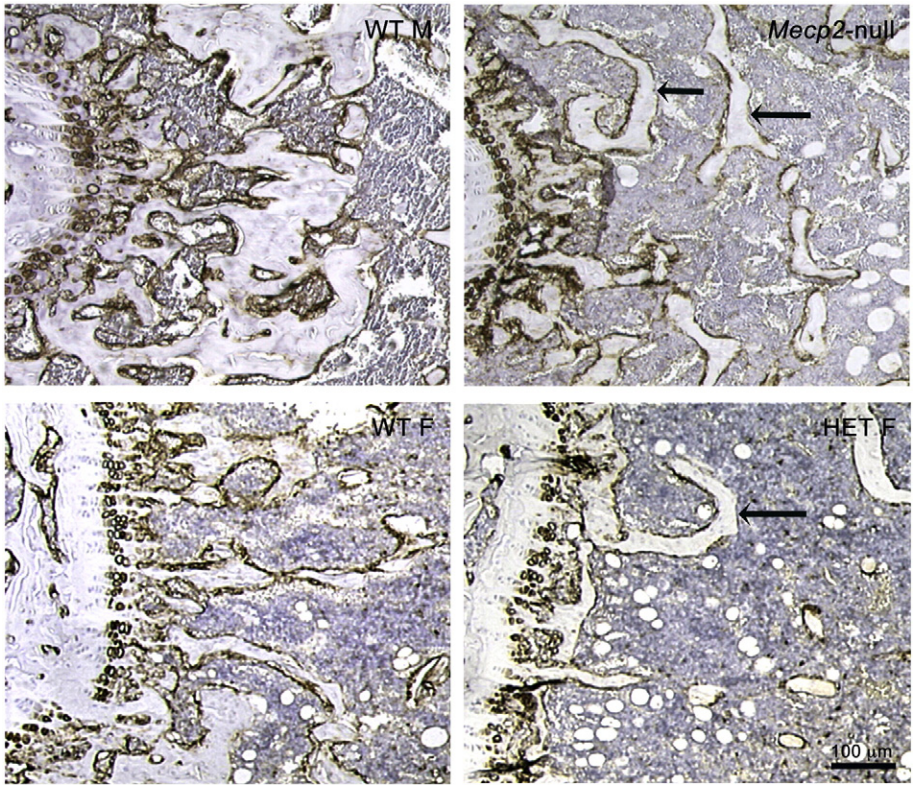

Fig. 3. Alkaline phosphatase staining is reduced in *Mecp2*-null and HET mice. Alkaline phosphatase staining was present at the growth plate and in osteoblasts in deeper trabeculae of WT M and WT F mice. In *Mecp2*-null male and in HET female mice, alkaline phosphatase staining was present at the growth plate but diminished compared to WT in the secondary spongiosa (black arrows; 5–7 mice were studied per group with 3 sections per bone sample examined).

growth plate and along the primary trabeculae just under the growth plate appeared normal in size and shape (Fig. 2). These cuboidal osteoblasts expressed procollagen I and were considered in an active state. However, in the secondary trabeculae (further from the growth plate) and along the endosteal surface, osteoblasts from *Mecp2*-null mice appeared very thin and small, similar in shape to "resting cells" that did not exhibit type I procollagen immunostaining (Fig. 2). The hypertrophic zone in the growth plate cartilage of femurs from WT, *Mecp2*-null and HET mice showed strong alkaline phosphatase activity. However, trabecular bone from *Mecp2*-null and HET mice had less alkaline phosphatase activity than from WT mice (Fig. 3).

Osteoblasts on secondary trabeculae in WT, *Mecp2*-null and HET mice were identified by immunostaining for type I procollagen. Osteoblast numbers were counted per 1 mm bone surface for *Mecp2*-null and WT male mice that were 5 weeks of age and for HET and WT female mice that were 12 weeks of age. The results showed that the number of osteoblasts was significantly reduced in both *Mecp2*-null (−44%) and HET (−28%) mice compared to their respective WT controls (Table 2).

TRAP stained osteoclasts were present in the femurs from 5 week-old WT and *Mecp2*-null male mice and from 13/14 week-old WT and HET female mice (data not shown). Counts of osteoclasts/mm bone surface did not show any significant differences among genotype groups (Table 2).

Dynamic parameters of bone growth were assessed following in vivo calcein and xylenol staining (Fig. 4). Mineral apposition rates (MAR; μ/day) were comparable in the WT male and female mice but were significantly decreased in both *Mecp2*-null and HET mice compared to respective WT mice ($p = <0.01$). Values for mineralizing surface/bone surface (double label + 1/2 single label/total surface) were significantly larger in WT females as compared to WT males. However, both *Mecp2*-null and HET mice had significantly lower values for mineralizing surface compared to their WT counterparts (p- < 0.001). Bone formation rates/surface (μ^3/μ^2/day) also were higher in the WT female than in the WT male but both *Mecp2*-null and HET mice had lower values compared to WT mice ($p = <0.0001$).

Osteoblast expression of MeCP2

In vitro cultures of osteoblasts from WT and *Mecp2*-null mice were immunostained with antibodies to MeCP2. The results showed that WT osteoblasts expressed MeCP2, while osteoblasts from *Mecp2*-null mice did not (Fig. 5). WT osteoblasts were slightly larger and had more cytoplasmic area, and the osteoblast layer was better organized than in *Mecp2*-null mice. In WT osteoblasts, MeCP2 was expressed predominantly in the nucleus, while in cerebellar granule cells, which serve as a positive staining control; MeCP2 was uniformly expressed throughout the cell soma.

Osteoblast growth in WT and Mecp2-null mice

These studies involved modeling growth curves over extended periods using crystal violet staining and fitting modified logistic curves [21]. Three parameters of the logistic that serve as markers for biologically relevant growth parameters were determined: 1) the plateau value or upper asymptote, which reflects the maximum cell density upon confluence, 2) lag time, which reflects the delay in time before cells enter into logarithmic growth and 3) the maximal growth rate, which is the inflection point on each fitted curve where the slope is maximized and represents the fastest growth rate. Bone cells derived from *Mecp2*-null mice consistently exhibited a higher maximal growth rate and higher final cell density, while their lag time was shorter than that observed in WT bone cells (Fig. 6).

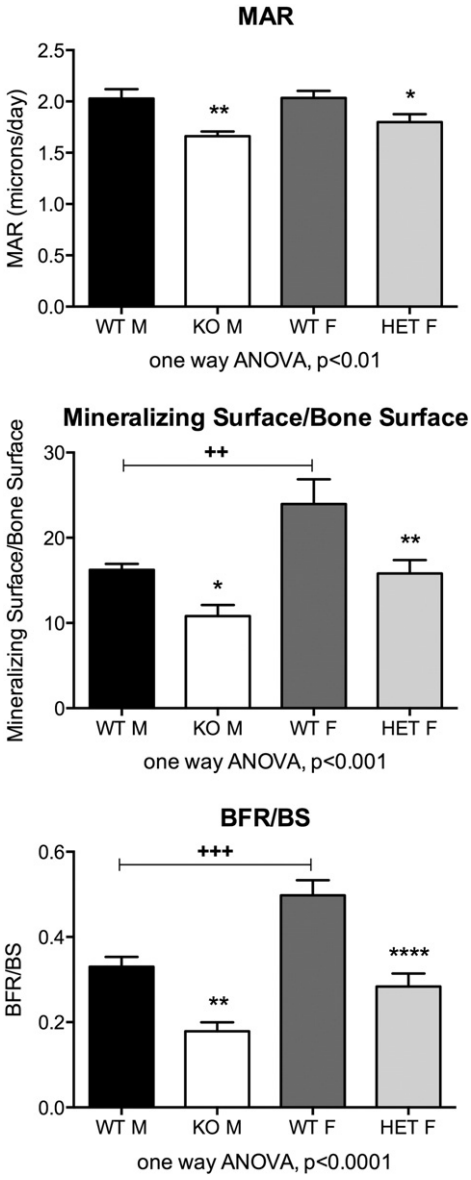

Fig. 4. Dynamic parameters of bone growth were altered in *Mecp2*-null and HET mice compared to WT males and females. Mineral apposition rates (MAR; μ/day; top panel) were significantly decreased in both *Mecp2*-null and HET mice compared to respective WT mice ($p \leq 0.01$). Values for mineralizing surface/bone surface (double label + 1/2 single label/total surface; middle panel) and bone formation rates/surface (BFR/BS; μ^3/μ^2/day; bottom panel) were significantly larger in WT females as compared to WT males. *Mecp2*-null and HET mice had significantly lower values for mineralizing surface compared to their WT counterparts (p- < 0.0010) and for bone formation ($p \leq 0.0001$). Values are the mean +/− SEM (n = 6–7 for each group).

Table 2
Osteoblast and osteoclast cell counts in *Mecp2*-null male and HET female mice versus age-matched WT male and female mice. Osteoblast cell numbers per mm bone surface were reduced in *Mecp2*-null and HET mice compared to respective WT mice. Osteoclast counts were standardized by dividing the number of osteoclasts by surface perimeter measured in millimeters. Osteoclast numbers were not reduced compared to WT.

Genotype	Osteoblast number	Osteoclast number
WT M	27.30 ± 1.92	4.44 ± 0.33
Mecp2-null M	15.30 ± 0.76*	4.96 ± 0.45
WT F	30.30 ± 1.39	7.45 ± 0.60
HET F	21.80 ± 1.57*	7.77 ± 0.67

* $p < 0.05$.

PCR

To further characterize the osteoblast function in *Mecp2*-null animals we compared mRNA expression for *Col1a1*, *Runx2* and *Osterix*

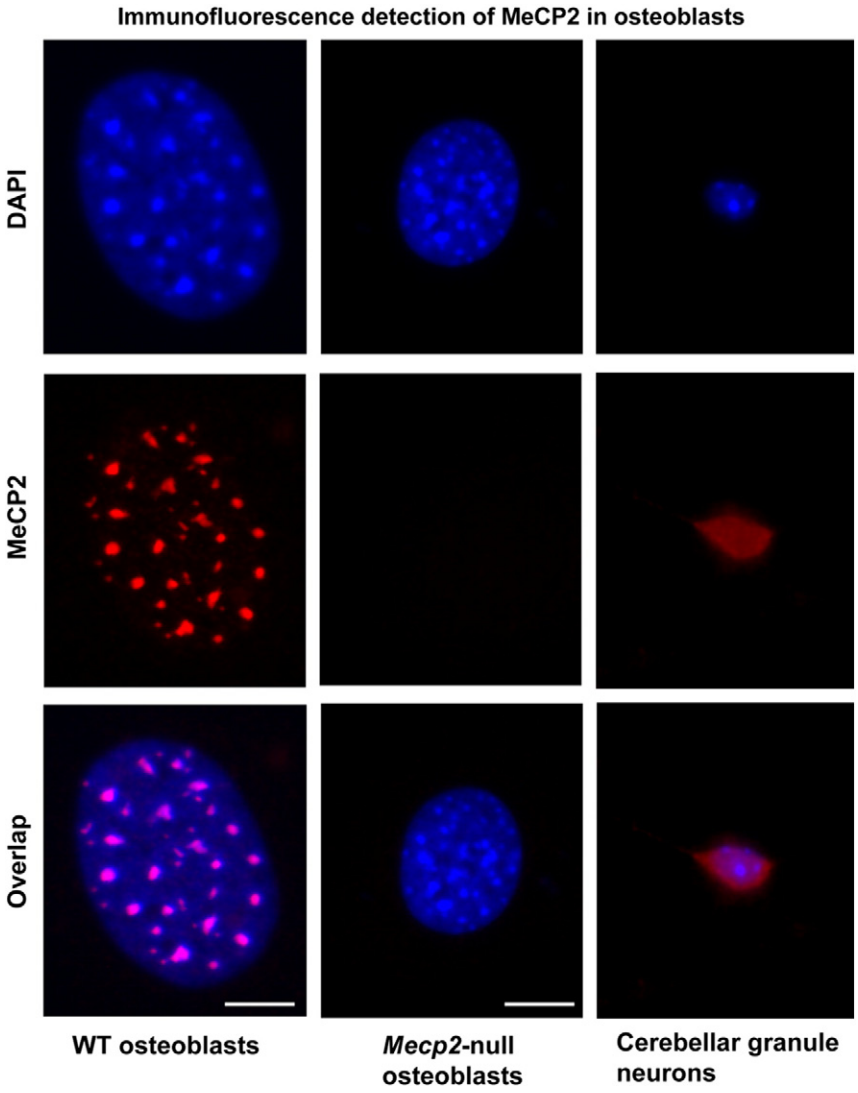

Fig. 5. Differential expression of MeCP2 in osteoblasts and cerebellar granule neurons cultured in vitro. Immunofluorescence with MeCP2 antibodies showed MeCP2 expression in osteoblasts from WT mice but not in osteoblasts from *Mecp2*-null mice. Cells were also stained with DAPI, which binds nucleic acid and labels cell nuclei (blue stain). MeCP2 was expressed in WT osteoblasts predominantly in their nucleoli, whereas in WT cerebellar granule cells, MeCP2 was expressed uniformly throughout the cell soma.

in WT versus *Mecp2*-null osteoblasts during 14 days in tissue culture (Fig. 7). The expression of *Col1a1* mRNA in *Mecp2*-null osteoblasts was lower than in the WT at day 10. The transcription factors *Runx2* and *Osterix* are major components of the Wnt–beta-catenin pathway [23]. Baseline *Runx2* mRNA expression was higher in *Mecp2*-null osteoblasts at early time points (days 3 and 6), compared with WT. At later time points (days 10 and 14), *Runx2* expression in the WT exceeded that in *Mecp2*-null cultures (Fig. 7). *Osterix* mRNA expression levels were lower at 3 and 6 day culture in *Mecp2*-null osteoblasts compared to WT but not at days 10 and 14 (Fig. 7).

Discussion

In 1997, Hass et al. reported that bone mineral content and spine bone mineral density were significantly reduced in a group of 20 subjects with RTT compared to both normal subjects and girls with cerebral palsy [5]. Another study found that 48.9% children and young adults with RTT had L1–L4 BMD values >2 SD below age-related norms [7]. Furthermore, this study showed that lumbar spine bone mineral content and bone mineral density (BMD) were correlated with weight, height, BMI, clinical severity, degree of scoliosis, use of anticonvulsants, and ambulatory status. Cuddapah et al. recently reported that specific *MECP2* mutations were associated with the severity of the neurologic disease [24]. However, in this and other reports, BMD did not correlate with a specific *MECP2* mutation [9,24]. Low bone mass and fractures occur at a relatively early age in children with RTT and thus it appears that these clinical factors do not fully explain the impact of the MeCP2 deficiency on the development of bone mass.

Osteoblast dysfunction has previously been implicated in the development of diminished bone mass in RTT syndrome. A 2003 histomorphometry study of tetracycline labeled iliac crest bone biopsies from 5 girls, ages 9 to 14 years showed that bone volume and osteoclast surface and number were reduced [10]. While the osteoid surface, one indicator of bone formation, was normal, the rate of bone formation was reduced in four/five girls. The authors quite rightly speculated that "perhaps *MECP2* mutations in Rett syndrome not only influence brain development but also affect bone formation" [10].

O'Connor et al. demonstrated a defect in osteoblast-derived bone formation in *Mecp2*-null mice compared to WT [11]. Dynamic histomorphometry revealed decreased mineral apposition rates (MAR) in femoral trabecular and calvarial bone, but not in cortical bone [11]. Our results confirm a decrease in MAR in *Mecp2*-null mice and extend those initial findings to HET females. In addition, decreases in bone formation rate and bone mineralizing surface in both *Mecp2*-

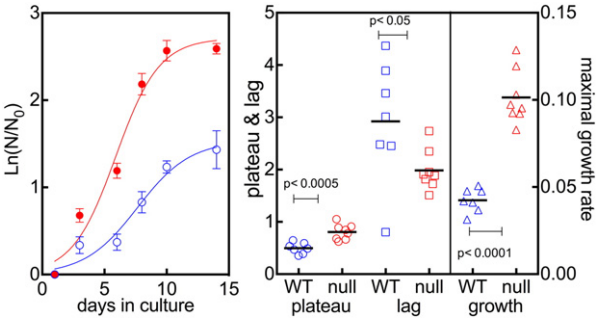

Fig. 6. Proliferation in *Mecp2*-null osteoblasts is more rapid than in the WT. Growth parameters kinetics were determined for 7 WT (blue; WT) and 8 *Mecp2*-null (red; null) osteoblast preparations. Osteoblasts from *Mecp2*-null mice had significantly increased growth rates (solid red circles-left panel) and higher plateau values (circles), and maximal growth rate (triangles) but lag time (squares) was shorter than in WT mice (right panel).

null and HET mice are consistent with osteoblast dysfunction. In contrast, TRAP staining demonstrated equivalent osteoclast number per mm bone surface in WT and *Mecp2*-null male mice. The alterations in both histology and dynamic parameters suggest that decreased bone mass in RTT is the result of a significant impact of MeCP2 deficiency on bone formation. Micro-CT data from *Mecp2*-null mice showed significant reductions in trabecular BV/TV, Tb.N, Tb.Th, and ConnD and increased Tb.Sp. All these changes are indicative of decreased bone mass in the *Mecp2*-null mice, and of a mechanically weaker and more fragile bone [25,26]. Cortical bone was less affected than trabecular bone, but there were significant reductions in BMD, Ct.Th and pMOI, each of which correlates with decreased mechanical strength [27].

Micro-CT parameters were diminished in HET compared to WT females but bone mass was not statistically decreased compared to WT. However, MAR, mineralizing rate and BFR were significantly decreased compared to WT females. These results differ from *Mecp2*-null mice in which both micro-CT and dynamic bone features were significantly decreased. It is possible that histomorphometric methods provide better spatial resolution than micro-CT, and therefore more sensitivity to detect more subtle differences. Alternatively, the presence of a normal X-chromosome in the HET females may modify specific parameters related to MAR and related functions with lesser impact on the absolute volume of bone mass measured by micro-CT. We

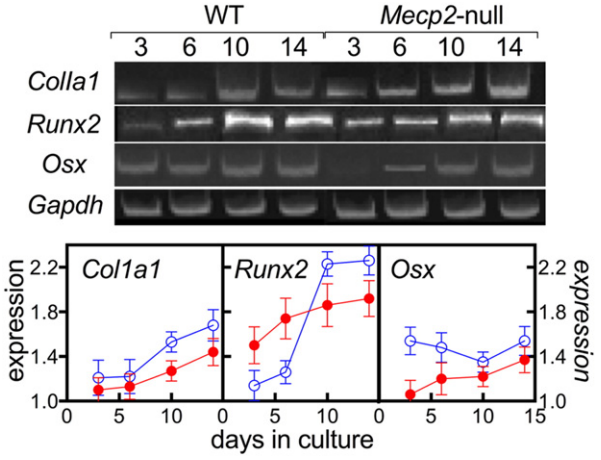

Fig. 7. Expression of osteoblast and osteogenic markers is altered in *Mecp2*-null osteoblasts. The RNA expression of type I collagen (*Col1a1*), *Runx2*, and *Osterix* (*Osx*) in WT and *Mecp2*-null (n = 3; mean +/− standard deviation) osteoblast cultures were profiled across days in culture for WT (blue) and *Mecp2*-null (red) osteoblasts. Expression values were normalized to *Gapdh*.

suggest that as in neural tissue, X-chromosome inactivation (XCI) is the major determinant of the extent of MeCP2 impact on osteoblast function. Both balanced and unbalanced XCI are known to substantially alter neural cell function and the same principle may apply for osteoblasts and other bone cells responsible for bone remodeling.

However, the lesser changes in bone mass in HET compared with *Mecp2*-null mice were not consistent with the bone loss seen at an early age in many young females with RTT. This thus suggests that ancillary clinical factors (nutrition, ambulation etc.) may aggravate bone loss to greater extent in humans than observed in female HET mice and also that other factors at the cellular level may moderate the extent of osteoblast impairment in HET mice. It also is possible that the age that we compared HET and WT female mice is too early to see a significant effect on bone mass. *Mecp2*-null mice express the neurodevelopmental disorder at a younger age and have a shorter life span compared to HET mice.

Osteoblast histomorphology and osteoblast number were altered in *Mecp2*-null and HET mice compared to respective WT controls. These results suggest that osteoblasts may be proliferating at a less than normal rate in the *Mecp2*-null mice, and are less active and less differentiated in secondary trabeculae and endosteum. In addition, the reductions in alkaline phosphatase activity in trabecular bone from HET mice are consistent with decreased osteoblast function [28].

In contrast to the histological findings, our in vitro results showed that osteoblasts from *Mecp2*-null mice cultured for 15 days had an increased growth rate and cell density compared to WT cells. However, cell culture beyond 15 days has not been completed so that a potential negative effect on osteoblast survival rate is not yet determined. In contrast, the effect of MeCP2 deficiency is well characterized in neuronal cells where deficiency leads to impaired neuronal maturation with severely retracted mature dendritic arbors of pyramidal neurons and dramatically reduced dendritic spine density [29]. Studies of brains from male hemizygous A140V mouse model revealed that a relative increase in cell packing density was due to overall decrease in neuronal size and a significant reduction in the complexity of neuronal dendritic branching [30]. An important issue involves a comparison of the negative effects of MeCP2 deficiency on the development of neural tissue with that in bone. Decreased expression of MeCP2 protein impairs synaptic and circuit maturation in the CNS and similarly impairs osteoblast function in bone [29,31]. Akin to multicellular neuronal interactions in the CNS, bone remodeling involves interactions among several cell types: osteoblasts, osteoclasts and osteocytes, where the role of MeCP2 deficiency requires definition for each cell type.

The mechanisms by which MeCP2 regulates gene expression remain only partially understood. MeCP2 represses gene transcription by histone deacetylase (HDAC)-dependent and HDAC-independent mechanisms each involving co-repressors such as SIM1 [32]. However, as shown in the mouse hypothalamus, MeCP2 also functions as a gene activator [3]. It has been suggested that MeCP2 targeted chromatin unfolding is central to expression of either activator or repressor activity [4]. The possibility exists that differences in MeCP2 function in neurons and osteoblasts involve epigenetic mechanisms leading to tissue-based specificity, here illustrated in the accelerated growth of the *Mecp2*-null-derived osteoblasts in vitro contrasted with the negative effect on neuronal development.

Conclusions

The results of this study using the Bird model of RTT provide new information related to impaired osteoblast function in the presence of MeCP2 deficiency. Micro-CT parameters showed a significant loss of trabecular and cortical bone mass in male *Mecp2*-null mice compared to WT, but no overall change was seen in female HET mice where dynamic bone parameters were decreased. Osteoblast morphology was altered in the presence of MeCP2 deficiency. In vivo cultured osteoblasts from *Mecp2*-null mice exhibited increased initial growth

rate but impaired mRNA expression of bone specific markers, *Col1A1*, *Runx2* and *Osterix*, after 15 days of culture. Thus, osteoblasts displayed the negative consequence of MeCP2 deficiency as observed in the central nervous system neurons in RTT. These results help to explain the occurrence of osteoporosis in children with RTT and may provide targets for future treatments.

Acknowledgments

We thank Charlotte Eyring (KKI) for her assistance with the mouse colony, genotyping and bone removal, Lyudmila Lukashova (HSS) for performing the micro-CT analysis and Orla O'Shea (HSS) for the histological evaluation. The International Rett Syndrome Foundation (#2910) and the Rett Syndrome Research Trust funded this work.

References

[1] Naidu S, Johnston MV. Neurodevelopmental disorders: clinical criteria for Rett syndrome. Nat Rev Neurol 2011;7:312–4.
[2] Amir RE, Van den Veyver IB, Wan M, Tran CQ, Francke U, Zoghbi HY. Rett syndrome is caused by mutations in X-linked MECP2, encoding methyl-CpG-binding protein 2. Nat Genet 1999;23:185–8.
[3] Chahrour M, Jung SY, Shaw C, Zhou X, Wong ST, Qin J, et al. MeCP2, a key contributor to neurological disease, activates and represses transcription. Science 2008;320:1224–9.
[4] Brink MC, Piebes DG, de Groote ML, Luijsterburg MS, Casas-Delucchi CS, van Driel R, et al. A role for MeCP2 in switching gene activity via chromatin unfolding and HP1gamma displacement. PLoS One 2013;8:e69347.
[5] Haas RH, Dixon SD, Sartoris DJ, Hennessy MJ. Osteopenia in Rett syndrome. J Pediatr 1997;131:771–4.
[6] Jefferson AL, Woodhead HJ, Fyfe S, Briody J, Bebbington A, Strauss BJ, et al. Bone mineral content and density in Rett syndrome and their contributing factors. Pediatr Res 2011;69:293–8.
[7] Shapiro JR, Bibat G, Hiremath G, Blue ME, Hundalani S, Yablonski T, et al. Bone mass in Rett syndrome: association with clinical parameters and MECP2 mutations. Pediatr Res 2010;68:446–51.
[8] Downs J, Bebbington A, Woodhead H, Jacoby P, Jian L, Jefferson A, et al. Early determinants of fractures in Rett syndrome. Pediatrics 2008;121:540–6.
[9] Roende G, Ravn K, Fuglsang K, Andersen H, Vestergaard A, Brondum-Nielsen K, et al. Patients with Rett syndrome sustain low-energy fractures. Pediatr Res 2011;69:359–64.
[10] Budden SS, Gunness ME. Possible mechanisms of osteopenia in Rett syndrome: bone histomorphometric studies. J Child Neurol 2003;18:698–702.
[11] O'Connor RD, Zayzafoon M, Farach-Carson MC, Schanen NC. Mecp2 deficiency decreases bone formation and reduces bone volume in a rodent model of Rett syndrome. Bone 2009;45:346–56.
[12] Guy J, Hendrich B, Holmes M, Martin JE, Bird A. A mouse *Mecp2*-null mutation causes neurological symptoms that mimic Rett syndrome. Nat Genet 2001;27:322–6.
[13] Metcalf BM, Mullaney BC, Johnston MV, Blue ME. Temporal shift in methyl-CpG binding protein 2 expression in a mouse model of Rett syndrome. Neuroscience 2006;139:1449–60.
[14] Verdelis K, Lukashova L, Atti E, Mayer-Kuckuk P, Peterson MG, Tetradis S, et al. MicroCT morphometry analysis of mouse cancellous bone: intra- and inter-system reproducibility. Bone 2011;49:580–7.
[15] Bouxsein ML, Boyd SK, Christiansen BA, Guldberg RE, Jepsen KJ, Muller R. Guidelines for assessment of bone microstructure in rodents using micro-computed tomography. J Bone Miner Res 2010;25:1468–86.
[16] Barka T, Anderson P. Histochemical methods for acid phosphatase used hexazonium pararosaniline as a coupler. J Histochem Cytochem 1962;10:741–52.
[17] Minkin C. Bone acid phosphatase: tartrate-resistant acid phosphatase as a marker of osteoclast function. Calcif Tissue Int 1982;34:285–90.
[18] Erben RG. Embedding of bone samples in methylmethacrylate: an improved method suitable for bone histomorphometry, histochemistry, and immunohistochemistry. J Histochem Cytochem 1997;45:307–13.
[19] Gruber HE. Adaptations of Goldner's Masson trichrome stain for the study of undecalcified plastic embedded bone. Biotech Histochem 1992;67:30–4.
[20] Vogiatzi MG, Tsay J, Verdelis K, Rivella S, Grady RW, Doty S, et al. Changes in bone microarchitecture and biomechanical properties in the th3 thalassemia mouse are associated with decreased bone turnover and occur during the period of bone accrual. Calcif Tissue Int 2010;86:484–94.
[21] Fedarko NS, D'Avis P, Frazier CR, Burrill MJ, Fergusson V, Tayback M, et al. Cell proliferation of human fibroblasts and osteoblasts in osteogenesis imperfecta: influence of age. J Bone Miner Res 1995;10:1705–12.
[22] Matsubara T, Kida K, Yamaguchi A, Hata K, Ichida F, Meguro H, et al. BMP2 regulates osterix through Msx2 and Runx2 during osteoblast differentiation. J Biol Chem 2008;283:29119–25.
[23] Stewart S, Gomez AW, Armstrong BE, Henner A, Stankunas K. Sequential and opposing activities of Wnt and BMP coordinate zebrafish bone regeneration. Cell Rep 2014;6:482–98.
[24] Cuddapah VA, Pillai RB, Shekar KV, Lane JB, Motil KJ, Skinner SA, et al. Methyl-CpG-binding protein 2 (MECP2) mutation type is associated with disease severity in Rett syndrome. J Med Genet 2014;51:152–8.
[25] Dalle Carbonare L, Giannini S. Bone microarchitecture as an important determinant of bone strength. J Endocrinol Invest 2004;27:99–105.
[26] Ulrich D, van Rietbergen B, Laib A, Ruegsegger P. The ability of three-dimensional structural indices to reflect mechanical aspects of trabecular bone. Bone 1999;25:55–60.
[27] Yao X, Carleton SM, Kettle AD, Melander J, Phillips CL, Wang Y. Gender-dependence of bone structure and properties in adult osteogenesis imperfecta murine model. Ann Biomed Eng 2013;41:1139–49.
[28] Silvent J, Nassif N, Helary C, Azais T, Sire JY, Guille MM. Collagen osteoid-like model allows kinetic gene expression studies of non-collagenous proteins in relation with mineral development to understand bone biomineralization. PLoS One 2013;8:e57344.
[29] Nguyen MV, Du F, Felice CA, Shan X, Nigam A, Mandel G, et al. MeCP2 is critical for maintaining mature neuronal networks and global brain anatomy during late stages of postnatal brain development and in the mature adult brain. J Neurosci 2012;32:10021–34.
[30] Jentarra GM, Olfers SL, Rice SG, Srivastava N, Homanics GE, Blue M, et al. Abnormalities of cell packing density and dendritic complexity in the MeCP2 A140V mouse model of Rett syndrome/X-linked mental retardation. BMC Neurosci 2010;11:19.
[31] Della Sala G, Pizzorusso T. Synaptic plasticity and signaling in Rett syndrome. Dev Neurobiol 2014;74:178–96.
[32] Gonzales ML, Adams S, Dunaway KW, LaSalle JM. Phosphorylation of distinct sites in MeCP2 modifies cofactor associations and the dynamics of transcriptional regulation. Mol Cell Biol 2012;32:2894–903.